Tetrahedron: *Asymmetry* 20 (2009) 1020–1026

Contents lists available at ScienceDirect

Tetrahedron: *Asymmetry*

journal homepage: www.elsevier.com/locate/tetasy

A DFT study of the enantioselective reduction of prochiral ketones promoted by pinene-derived amino alcohols

Donghui Wei, Mingsheng Tang *, Jing Zhao, Ling Sun, Wenjing Zhang, Chufeng Zhao, Shouren Zhang, Hongming Wang

Department of Chemistry, Center of Computational Chemistry, Zhengzhou University, Zhengzhou, Henan 450052, China

ARTICLE INFO

Article history:
Received 6 January 2009
Accepted 5 February 2009
Available online 23 April 2009

ABSTRACT

Recently, a pinene-derived amino alcohol [(1*R*,2*R*,3*S*,5*R*)-3-amino-2,6,6-trimethylbicyclo[3.1.1]heptan-2-ol] has been experimentally employed as an effective chiral catalytic precursor in the borane-mediated asymmetric reduction of prochiral ketones to produce the corresponding secondary alcohols, which provides the products in 96% ee. In this paper, we suggest a mechanism for this reduction process and then theoretically investigate it in detail by density functional theory. Fully geometry-optimized reactants, products, transition structures, and intermediates were obtained at the B3LYP/6-31G (d,p) level, and the results reveal that this reaction has five steps. Further calculations show that the solvent effect of THF has no great influence on the enantioselectivity of this reduction.

© 2009 Elsevier Ltd. All rights reserved.

1. Introduction

Since the first report by Itsuno[1] and further development by Corey[2] that enantiomerically pure oxazaborolidines efficiently catalyze the borane reduction of ketones to the corresponding secondary alcohols, numerous methodologies for the asymmetric reduction of ketones have been developed over the past decades, based on chiral reducing reagents or achiral ones. This is due to the challenges involved in such endeavors and is also due to the applications of homochiral secondary alcohols in organic and medicinal chemistry.[3–8] Much effort has been made in designing and developing various kinds of chiral catalysts.[9-24]

Recently, Hobuß et al. reported an experimental methodology employing pinene-derived amino alcohols, such as **1** (Scheme 1), as efficient chiral catalytic sources for the borane-mediated asymmetric reduction of prochiral ketones.[23] However, no report of theoretical investigations regarding the mechanism of the title reaction has been found.

We believe that the reaction utilizes the following mechanism:

All of the compounds shown in Scheme 1 will be referred to by their associated number for the sake of brevity. Initially **1** is converted successively into **1a** and **1b** (as can be seen in Scheme 1, **1a** is the true catalyst). The following processes, starting with the reaction between **1b** and the acetophenone, which are the reactants, are the focus of our investigation. The corresponding representation of the energy profile is illustrated in Figure 1.

2. Computational details

All theoretical calculations were performed using the GAUSSIAN 03[25] suite of programs. All structures were optimized by employing the hybrid density functional B3LYP method[26,27] and 6-31G (d,p) basis set. Vibrational frequency calculations were then performed at the optimized geometry of each reactant, product, transition structure, and intermediate. We confirmed that all reactants and intermediates have no imaginary frequencies, and each transition structure has one, and only one, imaginary frequency. The intrinsic reaction coordinate (IRC) calculations, at the same level of theory, were performed to ensure that the transition structures led to the expected reactants and products. Finally we have optimized the geometries of the two transition structures **TS2(*R*)** and **TS2(*S*)** in THF at the B3LYP/6-31G (d,p) level.

3. Results and discussion

We began by studying the chemical combination of **1b** with the acetophenone. It can be seen that **1b** can initiate the reaction through **TS1** (Fig. 2), which results from the approach of **1b** to the ketone and leads to the complex **M1** (Fig. 2). In **TS1**, the B2–O3 bond is 1.915 Å and the energy of **TS1** lies 3.90 kcal/mol above that of the reactants.

M1 lies 3.56 kcal/mol above the energy of the reactants. The interaction of the electron-deficient boron atom, B2, and the lone pair on O3 of the ketone stabilizes the resulting complexes (the B2–O3 distance is 1.688 Å in **M1**).

The second step is the transfer of H5 from the boron atom, B4, to the prochiral carbon atom, C6. The highly polarized carbonyl group

* Corresponding author.
E-mail address: donghuiwei6@163.com (M. Tang).

0957-4166/$ - see front matter © 2009 Elsevier Ltd. All rights reserved.
doi:10.1016/j.tetasy.2009.02.061

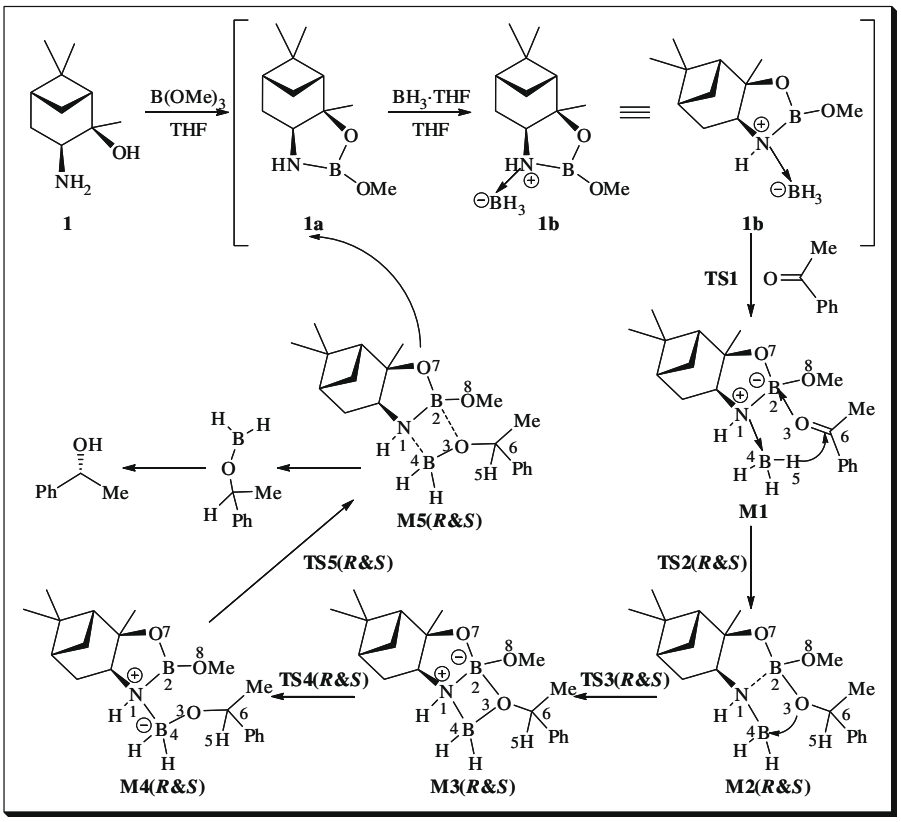

Scheme 1. The overall reaction mechanism.

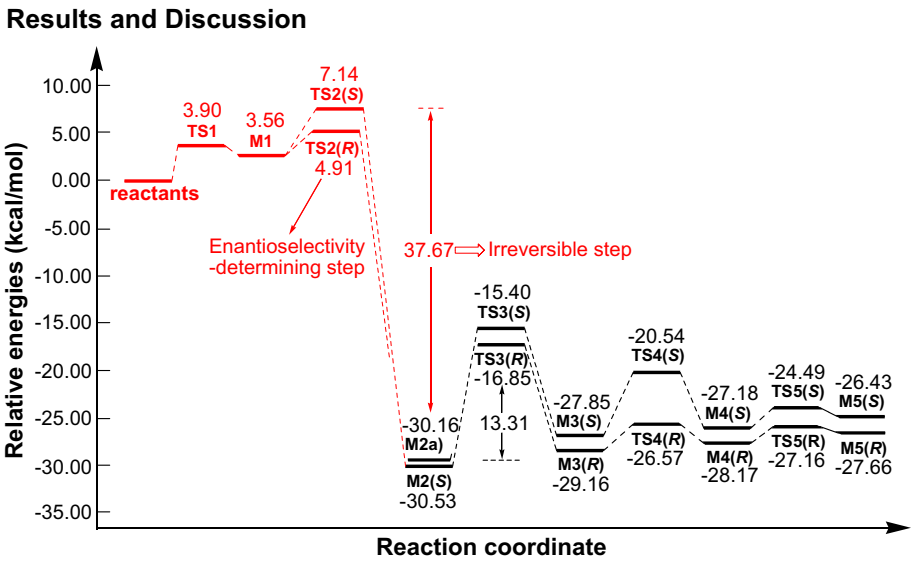

Figure 1. Potential energy profiles for the whole reaction along the reaction coordinate.

exhibits strong chemical reactivity, hence the carbon atom C6 is easily attacked by nucleophilic reagents.

In **M1**, the boron atom, B2, acts as a Lewis acid, which interacts with the O3 atom of the ketone. This type of interaction leads to a large increase in the positive charge on the C6 atom belonging to the carbonyl group. Hence, the likelihood of attack on the C6 atom by a nucleophilic reagent at this site is increased. One possible source of nucleophilic atoms is B4, which has three nucleophilic hydrogen atoms. Furthermore, the O3 atom exerts an influence upon the nearby H5 atom, one of the three hydrogen atoms of the B4 atom, making it more nucleophilic. As a result of above reasons, the H5 atom becomes the most nucleophilic among the three hydrogen atoms on B4 and is most easily transferred from the B4 atom to the electrophilic C6 atom. The transfer of the H5 atom in **M1**, corresponding to hydride attacking the *Re* face and *Si* face of the ketone, produces two diastereotopic transition structures **TS2(*R*)** and **TS2(*S*)**, respectively (Fig. 3).

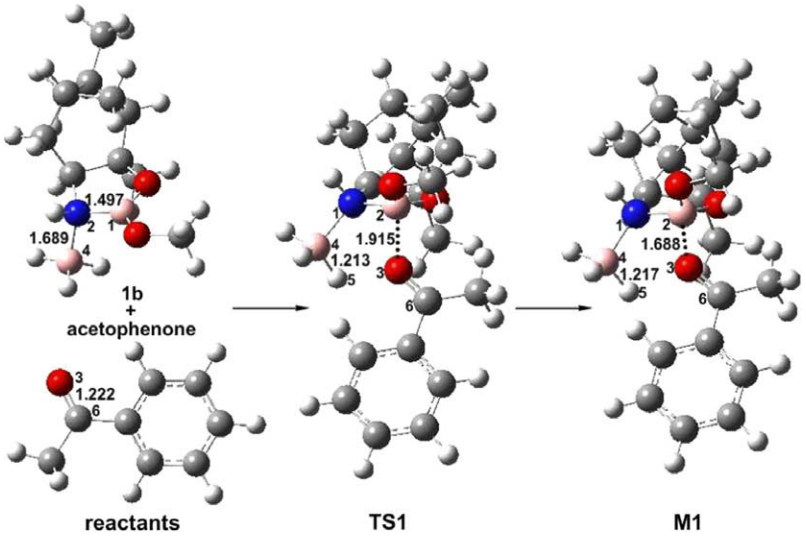

Figure 2. Optimized structures of the critical points reactants (**1b** and acetophenone), **TS1,** and **M1** (units in Å for bond lengths).

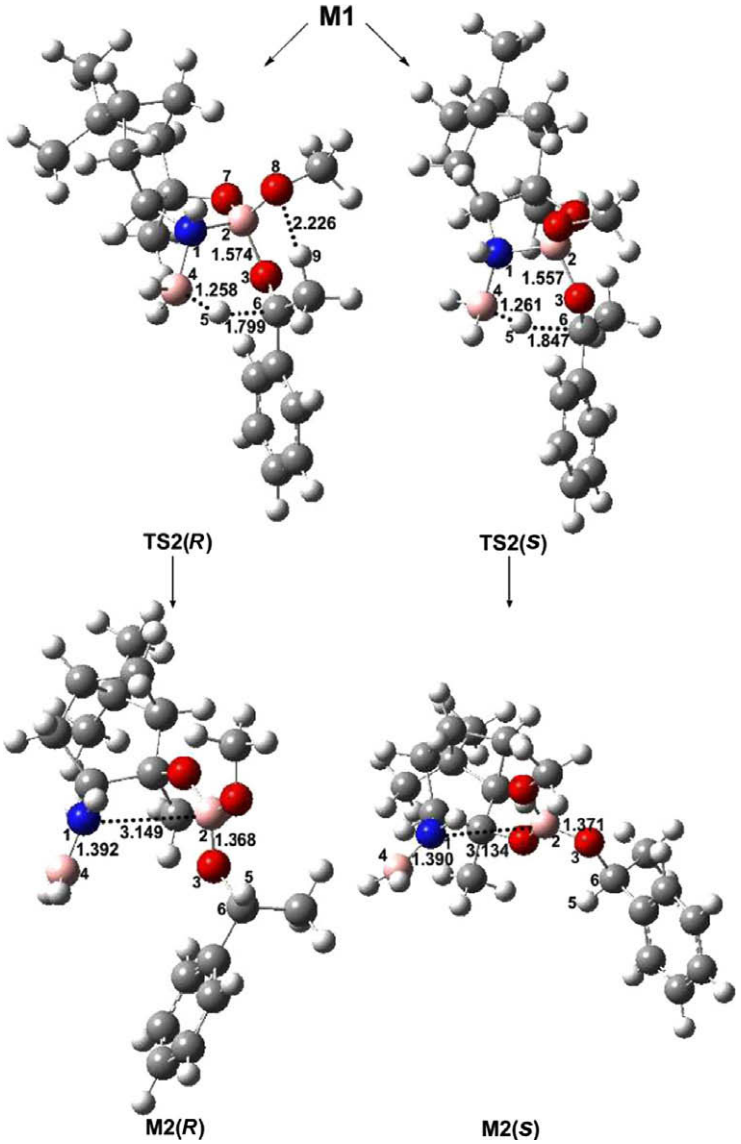

Figure 3. Optimized structures for **TS2(*R*&*S*)** and **M2(*R*&*S*)** (units in Å for bond lengths).

Table 1
Some geometrical parameters and RE (relative energies)[a] of some SP (stationary points) along the reaction channels (units in Å for bond lengths)

SP	B2···O3	B4···H5	H5···C6	RE
TS1	1.915	1.213	—	3.90
M1	1.688	1.217	—	3.56
TS2(*R*)	1.574	1.258	1.799	4.91
TS2(*S*)	1.557	1.261	1.847	7.14

[a] Values are energies relative to reactants and are given in kilocalories per mole.

Table 2
Some geometrical parameters and RE (relative energies)[a] of **M2(*R*&*S*)**, **TS3(*R*&*S*)**, **M3(*R*&*S*)**, **TS4(*R*&*S*)**, **M4(*R*&*S*)**, **TS5(*R*&*S*)**, and **M5(*R*&*S*)**

SP	N1···B2	B2···O3	O3···B4	B4···N1	RE
M2(*R*)	3.149	1.368	3.694	1.392	−30.16
M2(*S*)	3.134	1.371	—	1.390	−30.53
TS3(*R*)	2.309	1.437	1.860	1.462	−16.85
TS3(*S*)	2.378	1.433	1.824	1.466	−15.40
M3(*R*)	1.624	1.592	1.571	1.591	−29.16
M3(*S*)	1.584	1.635	1.561	1.600	−27.85
TS4(*R*)	1.536	2.061	1.502	1.639	−26.57
TS4(*S*)	1.463	2.261	1.413	1.559	−20.54
M4(*R*)	1.500	2.718	1.452	1.721	−28.17
M4(*S*)	1.508	2.699	1.462	1.675	−27.18
TS5(*R*)	1.455	3.173	1.385	2.167	−27.16
TS5(*S*)	1.468	2.944	1.398	2.035	−24.49
M5(*R*)	1.423	3.509	1.355	2.779	−27.66
M5(*S*)	1.420	3.863	1.348	3.004	−26.43

Units in Å for bond lengths.
[a] Values are energies relative to reactants and are given in kilocalories per mole.

In **TS2(*R*)**, the distance between C6 and H5 is 1.799 Å, while the breaking B4–H5 bond is 1.258 Å. The B2–O3 bond is shortened from 1.688 Å in the structure of **M1** to 1.574 Å in **TS2(*R*)**. The energy of **TS2(*R*)** is higher than that of the reactants by 4.91 kcal/mol, and **TS2(*R*)** leads to intermediate M2(*R*) that has an (*R*)-configuration at the stereogenic center, C6. **TS2(*S*)** leads to the (*S*)-configuration, **M2(*S*)**, and the newly forming C6–H5 bond is 1.847 Å, while the breaking B4–H5 bond is 1.261 Å. The energy of transition structure **TS2(*S*)** is 7.14 kcal/mol above the energy of the reactants. Similar to the case of **M1** and **TS2(*R*)**, the B2–O3 bond is shortened from 1.688 Å in **M1** to 1.557 Å in **TS2(*S*)**. The similarity in energy of these two transition structures can be mainly attributed to the similar stabilizing B2–O3 interaction (this distance is 1.574 Å in **TS2(*R*)** and 1.557 Å in **TS2(*S*)**, Table 1). The difference in energy between **TS2(*R*)** and **TS2(*S*)** is due to the different amount of repulsion between the ketone substituent closest to the catalyst and the functional groups on the catalyst. The repulsion is much weaker in **TS2(*R*)** than that in **TS2(*S*)**, because the distance between the closest ketone substituent and the catalyst in the former case is larger, according to the spacial structures of both transition structures. Furthermore, the O8 of the B-OMe group is important for stereoselectivity, because the hydrogen bond formed between the H9 of acetophenone and O8 of the catalyst [the distance is 2.226 Å in **TS2(*R*)**] lowers the energy barrier.

The two diastereomeric reduced complexes, **M2(*R*)** and **M2(*S*)** (Fig. 3), are found 30.16 and 30.53 kcal/mol below the energy of the reactants, respectively, indicating that the hydride transfer from B4 to C6 is exothermic. The energy barrier of **M2(*R*&*S*)** through **TS2(*R*&*S*)** is large (35.07 kcal/mol and 37.67 kcal/mol) and also indicates that the hydride transfer step is clearly irreversible at room temperature.[28] Hence the energy difference between **TS2(*R*)** and **TS2(*S*)** will be crucial to determine the stereochemical outcome of the reaction.

The energy difference between **TS2(*R*)** and **TS2(*S*)** is 2.23 kcal/mol. This value would correspond to an enantiomeric excess of about 96%, which predicts exactly the experimental outcome (96% ee). Thus, it provides the correct stereochemical preference to the reaction, in agreement with the experimental result.

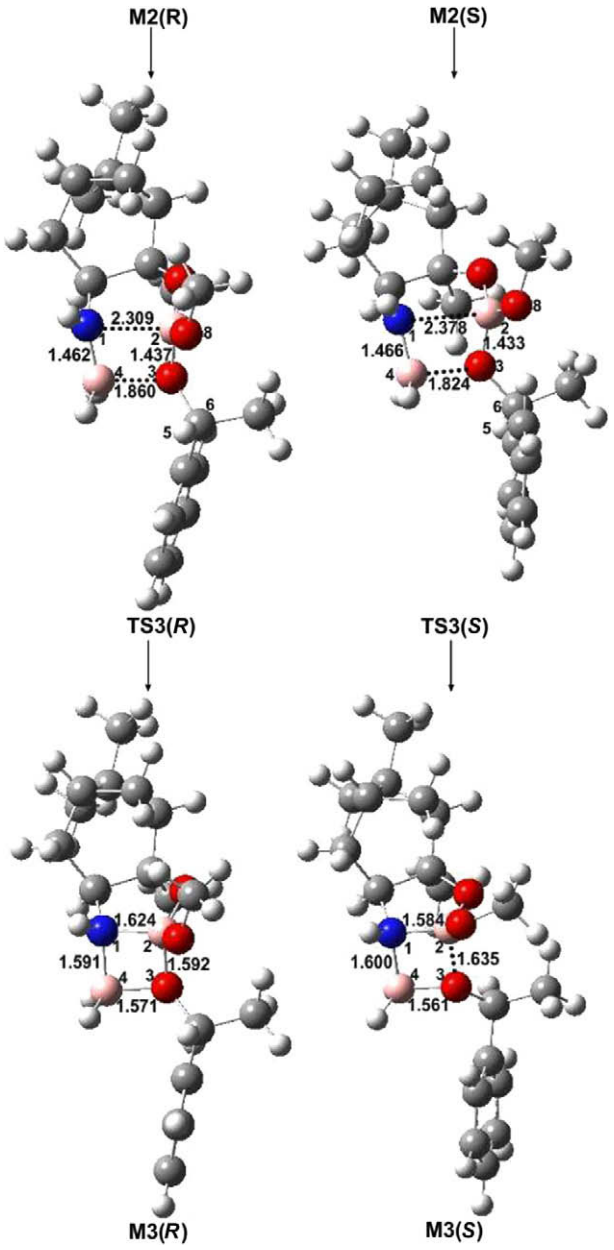

Figure 4. Optimized geometries of **TS3(*R*&*S*)** and **M3(*R*&*S*)** (units in Å for bond lengths).

After the hydride transfer, the five-membered heterocycle opens by breaking the N1–B2 bond. The distance between N1 atom and B2 atom reaches its maximum at intermediates **M2(*R*)** and **M2(*S*)** [3.149 Å and 3.134 Å in **M2(*R*&*S*)**]. At the same time, the bond lengths of the B2–O3 bond and the N1–B4 bond in **M2(*R*)** are shortened to 1.368 Å and 1.392 Å, respectively. Both bonds are shorter compared to 1.371 Å and 1.390 Å, respectively, in **M2(*S*)**.

In the process after the H5 transfer, the opened five-membered heterocycle in the catalyst is closed, and a four-membered ring (N1–B2–O3–B4) is formed through the [2+2] cycloaddition. The bond lengths of the N1–B4 and B2–O3 bonds increase from 1.392 Å and 1.368 Å in **M2(*R*)** to 1.462 Å and 1.437 Å in **TS3(*R*)**, which increase from 1.390 Å and 1.371 Å to 1.466 Å and 1.433 Å

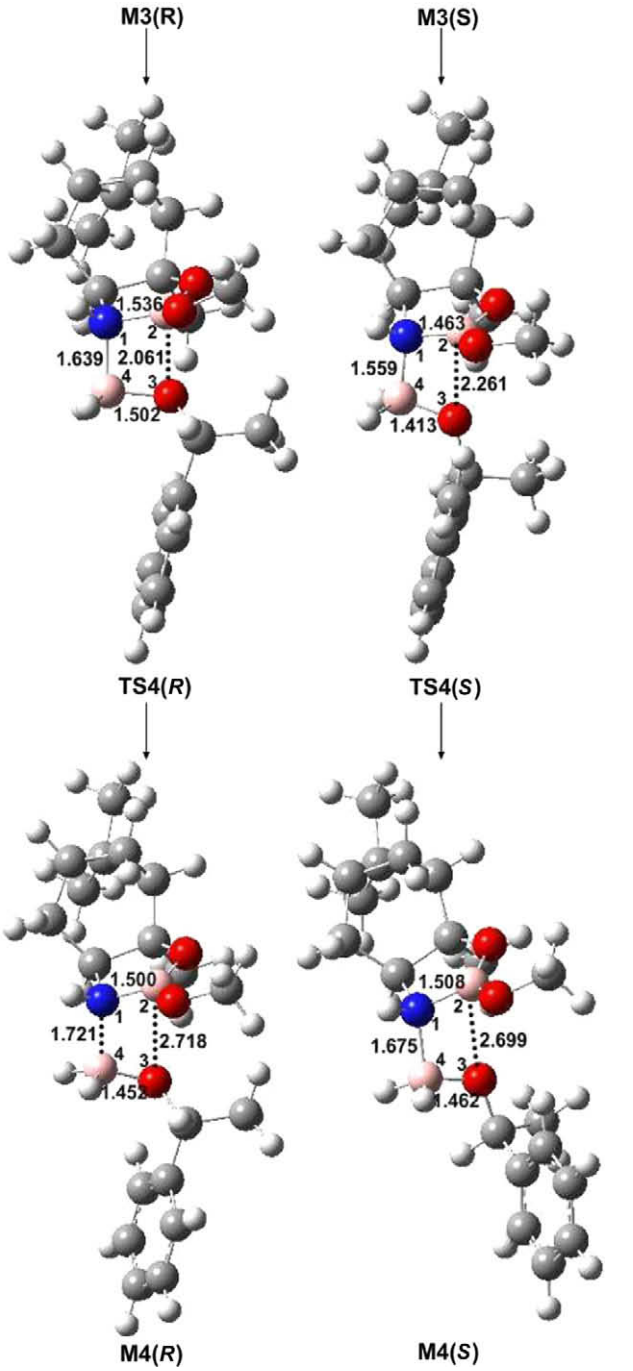

Figure 5. Optimized geometries of **TS4(*R*&*S*)** and **M4(*R*&*S*)** (units in Å for bond lengths).

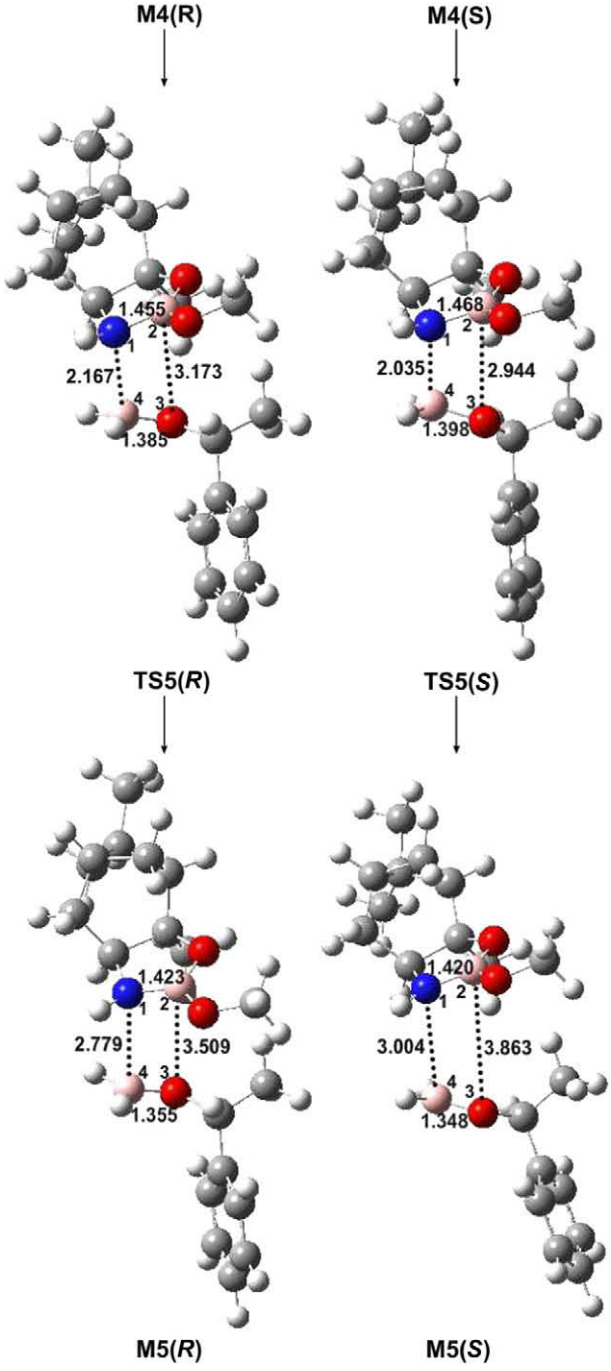

Figure 6. Optimized geometries of **TS5(*R*&*S*)** and **M5(*R*&*S*)** (units in Å for bond lengths).

in **TS3(*R*)** (Table 2). The lengthening of the N1–B4 and B2–O3 bonds is due to the change in coordination of the B2 (from tri-coordinated to tetra-coordinated). In **TS3(*R*)**, the distance between B2 and N1 is 2.309 Å, and the distance between O3 and B4 is 1.860 Å, while the B2–N1 and O3–B4 bond lengths are 2.378 Å and 1.824 Å in **TS3(*S*)** (Fig. 4). In **M3(*R*)**, the B2–N1 bond and the O3–B4 bond lengths change to 1.624 Å and 1.571 Å, which change to 1.584 Å and 1.561 Å in **M3(*S*)**, respectively. This change in bond lengths indicates that the B2–N1 and O3–B4 bonds are formed asymmetrically.

The barrier for ring formation is 13.31 kcal/mol through **TS3(*R*)** compared to 15.13 kcal/mol through **TS3(*S*)**. The energy of **M3(*R*&*S*)** is 29.16 and 27.85 kcal/mol lower than that of the reactants and 1.00 and 2.68 kcal/mol higher than that of **M2(*R*&*S*)**, which is mainly due to the strain in the newly formed four-membered ring.

In the last process of the reaction we considered, the four-membered ring (N1–B2–O3–B4) is opened and the oxaborane is released, by first breaking the B2–O3 bond through the transition structure **TS4(*R*&*S*)** leading to the complex **M4(*R*&*S*)** and then breaking the N1–B4 bond through **TS5(*R*&*S*)** to **M5(*R*&*S*)**. Why does the B2–O3 bond break first rather than the N1–B4 bond? We believe that the coordinate bond between the N and B atoms is stronger than the coordinate bond between the O and B atoms.

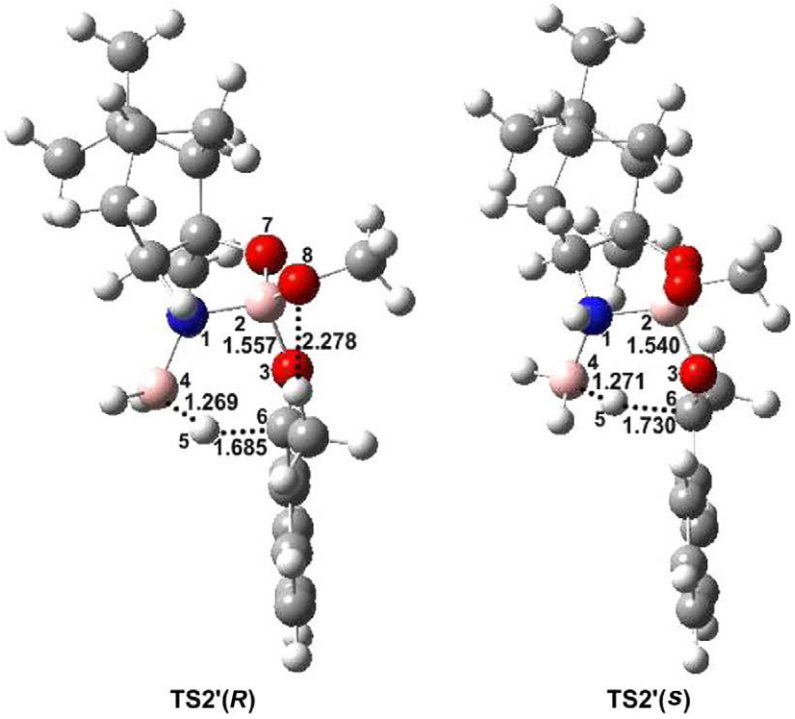

Figure 7. Optimized structures for **TS2′(*R*)** and **TS2′(*S*)** (units in Å for bond lengths).

The B2–O3 bond lengthens to 2.061 and 2.261 Å in **TS4(*R*&*S*)** and at last lengthens to 2.718 and 2.699 Å in **M4(*R*&*S*)** (Fig. 5), while the B2–N1 and O3–B4 bond lengths do not have a larger difference when compared to those in **M3(*R*&*S*)** (Table 2). Simultaneously, the N1–B4 bond lengthens from 1.639 and 1.559 Å in **TS4(*R*&*S*)** to 1.721 and 1.675 Å in **M4(*R*&*S*)**. The barrier through **TS4(*R*&*S*)** is 2.59 and 7.31 kcal/mol, so the B2–O3 bond will be broken easily leading to **M4(*R*&*S*)**.

Then the N1–B4 bond lengthens from 1.721 and 1.675 Å in **M4(*R*&*S*)** to 2.167 and 2.035 Å and is broken through the transition structure **TS5(*R*&*S*)** leading to the complex **M5(*R*&*S*)** (Fig. 6). **M5(*R*&*S*)** is now composed of two segments, the catalyst **1a** and the oxaborane that can be worked-up to form a secondary alcohol. In fact, the two segments still interact slightly with each other, since the N1–B4 distance is 2.779 and 3.004 Å and the B2–O3 distance is 3.509 and 3.863 Å. In **M5(*R*&*S*)**, the bond length of B2–N1 is 1.423 and 1.420 Å, nearly equal to the B2–N1 bond length in **1a**, implying that one segment of **M5(*R*&*S*)** is similar to the catalyst **1a** in its initial state. The O3–B4 bond decreases even more in going from **TS5(*R*&*S*)** to **M5(*R*&*S*)** with a final value of 1.355 and 1.348 Å. The barrier through **TS5(*R*&*S*)** is 1.01 and 2.69 kcal/mol, so the N1–B4 bond will also be broken easily leading to **M5(*R*&*S*)**. The energy of **M5(*R*&*S*)** is 27.66 and 26.43 kcal/mol lower than that of the reactants, therefore, the overall reaction is an exothermic process. Though the intermediates **M2(*R*)** and **M2(*S*)** are the most stable points on the potential energy profiles, the whole reaction is a dynamic process and the energy barrier is so low that the intermediates **M2(*R*)** and **M2(*S*)** can easily transform to the intermediates **M5(*R*)** and **M5(*S*)**.

The solvent effect of THF on the enantioselectivity of this reduction was also taken into account. We have computed the two transition structures **TS2(*R*)** and **TS2(*S*)** in THF, using the PCM method by means of geometrical optimizations. The structures of these are **TS2′(*R*)**, **TS2′(*S*)**, and are represented in Figure 7. The energy difference between **TS2′(*R*)** and **TS2′(*S*)** is 2.00 kcal/mol compared to 2.23 kcal/mol between **TS2(*R*)** and **TS2(*S*)**, there is almost no difference in the solvent.

4. Conclusions

In this paper an integrated mechanism for the catalytic reduction of acetophenone has been investigated using density functional theory (DFT). The results reveal that this reduction takes place via five steps: initially **1b** approaches the carbonyl group of the ketone. The second step is a hydride transfer, which can occur via two different pathways, and each has a diastereotopic transition structure. One pathway corresponds to attack of the hydride at the *Re* face while the other pathway involves attack at the *Si* face. Our calculations indicate that the stereoisomer with the (*R*)-configuration at the new chiral center is significantly more energetically favorable. The energetic favorability of the (*R*)-configured stereoisomer suggests that it should be the dominant product, which is in good agreement with experiment. In addition, as shown by the potential energy profile (Fig. 1), the transition structures of hydride transfer are key for stereoselectivity. The remaining three steps involve closure of the five-membered ring of the catalyst and release of the oxaborane. The first step occurs through a [2+2] cycloaddition to give rise to a new four-membered ring, and in the latter two steps, oxaborane is released by stepwise breaking of two bonds of the four-membered ring. The calculations also indicate that the solvent effect of THF has not influenced greatly the enantioselectivity of this reduction.

Acknowledgment

The work described in this paper was supported by the National Natural Science Foundation of China (No. 20672104).

References

1. (a) Hirao, A.; Itsuno, S.; Nakahama, S.; Yamazaki, N. *J. Chem. Soc., Chem. Commun.* **1981**, *7*, 315–317; (b) Itsuno, S.; Ito, K.; Hirao, A.; Nakahama, S. *J. Chem. Soc., Chem. Commun.* **1983**, *8*, 469–470; (c) Itsuno, S.; Ito, K.; Hirao, A.; Nakahama, S. *J. Org. Chem.* **1984**, *49*, 555–557.

2. (a) Corey, E. J.; Bakshi, R. K.; Shibata, S.; Chen, C.-P.; Singh, V. K. *J. Am. Chem. Soc.* **1987**, *109*, 7925–7926; (b) Corey, E. J.; Bakshi, R. K.; Shibata, S. *J. Am. Chem. Soc.* **1987**, *109*, 5551–5553; (c) Corey, E. J.; Bakshi, R. K.; Shibata, S. *J. Org. Chem.* **1988**, *53*, 2861–2863.
3. Brown, H. C.; Jadhav, P. K.; Singaram, B. *Mod. Synth. Meth.* **1986**, *4*, 307–356.
4. Brown, H. C.; Ramachandran, P. V. *Acc. Chem. Res.* **1992**, *25*, 16–24.
5. Singh, V. K. *Synthesis* **1992**, *7*, 607–617.
6. Wallbaum, S.; Martens, J. *Tetrahedron: Asymmetry* **1992**, *3*, 1475–1504.
7. Deloux, L.; Srebnik, M. *Chem. Rev.* **1993**, *93*, 763–784.
8. (a) Corey, E. J.; Guzman-Perez, A.; Lazerwith, S. E. *J. Am. Chem. Soc.* **1997**, *119*, 11769–11776; (b) Corey, E. J.; Helal, C. J. *Angew. Chem., Int. Ed.* **1998**, *37*, 1986–2012.
9. Quallich, J. G.; Blake, J. F.; Woodall, T. M. *J. Am. Chem. Soc.* **1994**, *116*, 8516–8525.
10. Giffels, G.; Dreisbach, C.; Kragl, U.; Weigerding, M.; Waldmann, H.; Wandrey, C. *Angew. Chem., Int. Ed. Engl.* **1995**, *34*, 2005–2006.
11. Gamble, M. P.; Smith, A. R. C.; Wills, M. *J. Org. Chem.* **1998**, *63*, 6068–6071.
12. Goldfuss, B.; Houk, K. N. *J. Org. Chem.* **1998**, *63*, 8998–9006.
13. Puigjaner, C.; Vidal-Ferran, A.; Moyano, A.; Pericàs, M. A.; Riera, A. *J. Org. Chem.* **1999**, *64*, 7902–7911.
14. Sarvary, I.; Almqvist, F.; Frejd, T. *Chem. Eur. J.* **2001**, *7*, 2158–2166.
15. Hu, J.-b.; Zhao, G.; Yang, G.-s.; Ding, Z.-d. *J. Org. Chem.* **2001**, *66*, 303–304.
16. Hu, J.-b.; Zhao, G.; Ding, Z.-d. *Angew. Chem., Int. Ed.* **2001**, *40*, 1109–1111.
17. Du, D.-M.; Fang, T.; Xu, J.; Zhang, S.-W. *Org. Lett.* **2006**, *8*, 1327–1330.
18. (a) Stepanenko, V.; Ortiz-Marciales, M.; Correa, W.; De Jesús, M.; Espinosa, S.; Ortiz, L. *Tetrahedron: Asymmetry* **2006**, *17*, 112–115; (b) Stepanenko, V.; De Jesus, M.; Correa, W.; Guzman, I.; Vazquez, C.; De la Cruz, W.; Ortiz-Marciales, M.; Basnes, C. L. *Tetrahedron Lett.* **2007**, *48*, 5799–5802.
19. (a) Basavaiah, D.; Jayapal Reddy, G.; Chandrashekar, V. *Tetrahedron: Asymmetry* **2001**, *12*, 685–689; (b) Basavaiah, D.; Jayapal Reddy, G.; Chandrashekar, V. *Tetrahedron: Asymmetry* **2002**, *13*, 1125–1128; (c) Basavaiah, D.; Jayapal Reddy, G.; Chandrashekar, V. *Tetrahedron: Asymmetry* **2004**, *15*, 47–52; (d) Basavaiah, D.; Jayapal Reddy, G.; Venkateswara Rao, K. *Tetrahedron: Asymmetry* **2004**, *15*, 1881–1888; (e) Basavaiah, D.; Chandrashekar, V.; Das, U.; Jayapal Reddy, G. *Tetrahedron: Asymmetry* **2005**, *16*, 3955–3962; (f) Basavaiah, D.; Venkateswara Rao, K.; Sekhara Reddy, B. *Tetrahedron: Asymmetry* **2006**, *17*, 1036–1040; (g) Basavaiah, D.; Venkateswara Rao, K.; Sekhara Reddy, B. *Tetrahedron: Asymmetry* **2006**, *17*, 1041–1044; (h) Basavaiah, D.; Venkateswara Rao, K.; Sekhara Reddy, B. *Tetrahedron: Asymmetry* **2007**, *18*, 968–974.
20. Wills, M.; Gamble, M.; Palmer, M.; Smith, A.; Studley, J.; Kenny, J. *J. Mol. Catal. A* **1999**, *146*, 139–148.
21. Masui, M.; Shioiri, T. *Synlett* **1997**, *3*, 273–274.
22. (a) Xu, J. X.; Wei, T. Z.; Zhang, Q. H. *J. Org. Chem.* **2003**, *68*, 10146–10151; (b) Xu, J. X.; Wei, T. Z.; Zhang, Q. H. *J. Org. Chem.* **2004**, *69*, 6860–6866.
23. Hobuß, D.; Baro, A.; Laschat, S.; Frey, W. *Tetrahedron* **2008**, *64*, 1635–1640.
24. Sun, L.; Tang, M.-S.; Wang, H.-m.; Wei, D.-h.; Liu, L.-l. *Tetrahedron: Asymmetry* **2008**, *19*, 779–787.
25. Frisch, M. J.; Trucks, G. W.; Schlegel, H. B.; Scuseria, G. E.; Robb, M. A.; Cheeseman, J. R.; Montgomery, J. A..; Vreven, T., Jr.; Kudin, K. N.; Burant, J. C.; Millam, J. M.; Iyengar, S. S.; Tomasi, J.; Barone, V.; Mennucci, B.; Cossi, M.; Scalmani, G.; Rega, N.; Petersson, G. A.; Nakatsuji, H.; Hada, M.; Ehara, M.; Toyota, K.; Fukuda, R.; Hasegawa, J.; Ishida, M.; Nakajima, T.; Honda, Y.; Kitao, O.; Nakai, H.; Klene, M.; Li, X.; Knox, J. E.; Hratchian, H. P.; Cross, J. B.; Bakken, V.; Adamo, C.; Jaramillo, J.; Gomperts, R.; Stratmann, R. E.; Yazyev, O.; Austin, A. J.; Cammi, R.; Pomelli, C.; Ochterski, J. W.; Ayala, P. Y.; Morokuma, K.; Voth, G. A.; Salvador, P.; Dannenberg, J. J.; Zakrzewski, V. G.; Dapprich, S.; Daniels, A. D.; Strain, M. C.; Farkas, O.; Malick, D. K.; Rabuck, A. D.; Raghavachari, K.; Foresman, J. B.; Ortiz, J. V.; Cui, Q.; Baboul, A. G.; Clifford, S.; Cioslowski, J.; Stefanov, B. B.; Liu, G.; Liashenko, A.; Piskorz, P.; Komaromi, I.; Martin, R. L.; Fox, D. J.; Keith, T.; Al-Laham, M. A.; Peng, C. Y.; Nanayakkara, A.; Challacombe, M.; Gill, P. M. W.; Johnson, B.; Chen, W.; Wong, M. W.; Gonzalez, C.; Pople, J. A. GAUSSIAN *03, Revision C.02*; Gaussian, Wallingford CT, 2004.
26. Becke, A. D. *J. Chem. Phys.* **1993**, *98*, 5648–5652.
27. Lee, C.; Yang, W.; Parr, R. G. *Phys. Rev. B* **1988**, *37*, 785–789.
28. Bandini, M.; Bottoni, A.; Cozzi, P. G.; Miscione, G. P.; Monari, M.; Pierciaccante, R.; Umani-Ronchi, A. *Eur. J. Org. Chem.* **2006**, *20*, 4596–4608.